

Topological Invariants in Invasion Percolation

Fernando Alonso-Marroquin*

CIPR, King Fahd University of Petroleum and Minerals, Dhahran, 31261, Kingdom of Saudi Arabia.

(Dated: May 8, 2025)

Based on a graph morphology algorithm of invasion percolation, the relationship between capillary pressure and saturation during drainage is calculated. Two topological invariants are identified: The bond percolation threshold and the residual saturation. Bond percolation with trapping is employed to derive a closed-form pressure-saturation relation, expressed in terms of the pore geometry (pore throat distribution) and material parameters (contact angle and interfacial tension), as well as universal exponents and topological invariants, all connected according to scaling relations. The simulations suggest that the exponents of these scaling relations, along with the power-law relations between residual saturation and lattice size, are universal. Conversely, the self-similar relations are non-universal, and the self-similar function of the supercritical regime is governed by the coordination number of the lattice.

Keywords: capillary flow, multiphase flow, porous media

The movement of one fluid, displacing another in a porous medium, appears in various fields, such as physics [1], geology [2], hydrology [3], and social sciences [4]. Understanding this process, known as invasion percolation [5], is of paramount importance. Our daily productivity depends on two factors: (1) whether hot water can pass through ground coffee in our coffee machine, and (2) how efficiently hot water extracts the richness of the coffee compounds. The first factor is controlled by the percolation threshold, while the second is related to residual saturation. This letter demonstrates that these two quantities are topological invariants—they do not depend on the material properties or the geometry of the porous medium. Instead, they depend solely on the topology of the porous network and can be derived from percolation theory.

Percolation is one of the most documented emerging phenomena in complex systems. It appears when the nodes or bonds in a random network are progressively activated, creating connected clusters where complex patterns emerge [1, 4]. In bond percolation theory, the control parameter p is defined as the probability of bond occupancy in a network. A phase transition occurs at a critical value p_c . Above this value, large-scale connectivity begins to emerge in the lattice. Perhaps the most exciting theoretical advance on bond percolation is the Kesten theorem [6] that provides a rigorous demonstration that the bond percolation threshold for infinite-square lattices is $p_c = 1/2$. Kersten theorem confirmed previous analytical derivations by Sykes and Essan, who also showed bond percolation threshold of $2 \sin(\pi/18)$, $1/2$, $1 - 2 \sin(\pi/18)$ and for triangular, rectangular, and honeycomb lattices [7]. Far less theoretical advances have been presented on invasion percolation. To date, it is still not clear how the percolation transition and the residual saturation in invasion percolation are related to the topology and morphology of the porous media and the

material parameters of the pores and fluids. It is unclear whether the transition is connected to classical percolation, backbone percolation transition, or whether it is a new kind of transition [2]. The transition is often associated with the backbone percolation threshold, which is not a topological invariant [8]. Residual saturation depends on many factors, such as wettability and capillary number [9–11], but it is unknown how residual saturation upon primary drainage is related to material properties in the quasi-static limit. This Letter closes this gap by using bond percolation theory to relate capillary pressure-saturation relations to topological invariants, pore throat distribution, and interfacial properties of solids and liquids.

In invasion percolation (IP), it is assumed that the porous medium is initially filled with a resident fluid, and it is progressively invaded by another fluid in an immiscible and incompressible fashion [12]. The porous medium is modeled as a network of spherical pores connected by cylindrical throats. Blunt [13] presented the connection between IP during drainage and bond percolation (BP). There, the quasi-static displacement of the liquid in a throat of radius r is resolved by the equilibrium between capillary forces $P_c \times \pi r^2$ and surface tension $\gamma \cos \theta \times 2\pi r$, where P_c is the capillary pressure, γ and θ are the interfacial tension and the contact angle. Thus, the capillary pressure required to invade the throat $P_c = 2\gamma \cos \theta / r$. For a given capillary pressure, the *potentially active* throats are defined as these whose radius satisfies $r > r_c$, where r_c is the so-called *capillary radius*:

$$r_c = \frac{2\gamma \cos \theta}{P_c} \quad (1)$$

To establish the link between quasi-static IP and BP, the undirected graph of the pore network g is defined as the collection of all pores (nodes) and throats (edges). In the same way, we define the *allowed graph* from the subset $g_0 \subseteq g$ of all potentially active throats, that is, the subset of the graph that can potentially be invaded. g_0 defines the pore space that can potentially be invaded,

* fernando@quantumfi.net

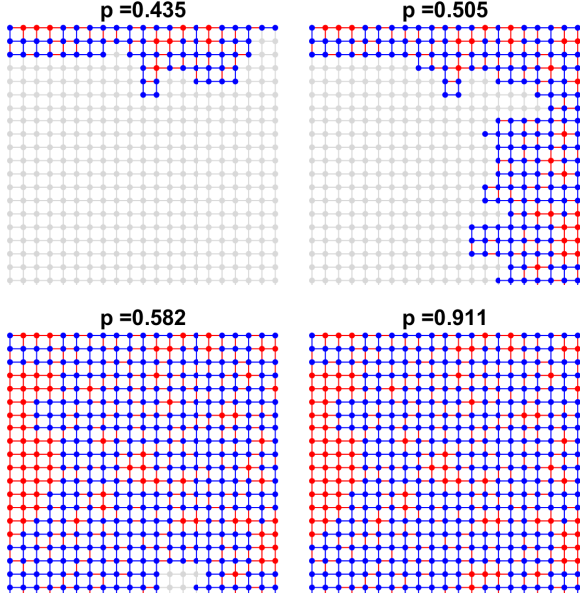


FIG. 1. Snapshots of the lattice invasion on a square lattice. The defended, invaded, and trapped phases are represented by gray, blue, and red colors, respectively. The first snapshot corresponds to the subcritical regime, $p < p_c$. The second snapshot is taken around the critical threshold, $p \approx p_c$. The third snapshot captures the moment when the invaded network is fully established, and the last snapshot shows the final stage of drainage. The top/bottom nodes are connected to the injection/evacuation zone.

that is distinct to the pore space that is actually occupied [14]. Whether this grain can be invaded depends on the connectivity between the invading and defending fluids and the injection/evacuation pores. For the purpose of simulating the invasion percolation, Blunt [13] defines occupancy as the fraction of throats that belong to g_0 , that is, $p = N_0/N_T$, where N_0 is the number of active bonds and N_T is the total number of bonds. based on Eq. 1, the occupation probability can be calculated in terms of the cumulative distribution function of the throat radii $F(r)$ as:

$$p = 1 - F(r_c). \quad (2)$$

Eq. 2 leads to a beautiful parallel between quasi-static IP and BP, where percolation is controlled by the occupation probability p . A percolation threshold p_c is expected, above which a phase transition occurs, leading to the emergence of a giant connected component in the pore network. The order parameter in bond percolation is typically defined as the probability that a given node belongs to the largest cluster [6]. In our case, it is more convenient to use another order parameter that is the saturation; This is defined as the fraction of pores that are invaded, $S_I = N_{p,I}/N_p$. Since we simulate drainage, all the nodes connected to the invaded throats are invaded.

The invasion percolation algorithm presented here is an improved version of the Hilper & Miller's pore mor-

phology method (PMM) [15, 16]. The PMM calculates the invasion based on morphological operations and connectivity functions on the binary image of the porous medium. Here, an improvement of the method is proposed by formulating the problem on the undirected graph instead. First, the morphological erosion and connectivity operator for the undirected graph is defined as follows: The erosion of a graph $g_0 = g \ominus S_r$ is the subset of g that contains only the throats whose radii are larger than r ; the connectivity function $g_c = C(g_1, g_2)$ returns the graph of the connected components of g_1 that are connected to g_2 . The computational complexity of these operations is $O(zN)$, where $z = N_t/N_p$ is the average coordination number, and N_t and N_p is the number of throats and pores.

To include residual saturation in the algorithm, the defended pore space that gets disconnected from the evacuation zone is considered as *trapped* during the drainage. With this aim, the graph is assumed to be a partition of three subgraphs: the defended g_D , the invaded g_I , and the trapped g_T : $g = g_I \cup g_D \cup g_T$. The drainage condition implies that the nodes connected to the invaded graph are added to it; see Figure 1. As boundary conditions, some of the graph nodes are assumed to be connected to the reservoir (R) where the invasive fluid is injected, and some of the nodes are connected to the evacuation zone (E) where the resident fluid escapes. For the initial condition, the entire graph corresponds to the defended graph and the capillary pressure is zero. Each step of the quasistatic simulation is implemented as follows:

1. The occupancy p is incremented, and the capillary radius r_c is calculated using Eq. 2.
2. The capillary pressure P_c is calculated from Eq. 1.
3. The allowed graph is calculated as $g_0 = g \ominus S_{r_c}$; The nodes connected to g_0 are added to it.
4. The part of the g_0 that is not trapped and is connected to the reservoir is added to the invaded graph. $g_{new}^I = C(g_0 - g_T, R)$; $g_I \leftarrow g_I \cup g_{new}^I$.
5. The defended graph is calculated as the graph that is not invaded and is connected to the evacuation zone. $g_D = C(g - g_I, E)$.
6. The graph that is neither invaded nor defended is added to the trapped graph. $g_{new}^T = g - (g_D \cup g_I)$; $g_T \leftarrow g_T \cup g_{new}^T$.
7. Return to Step 1.

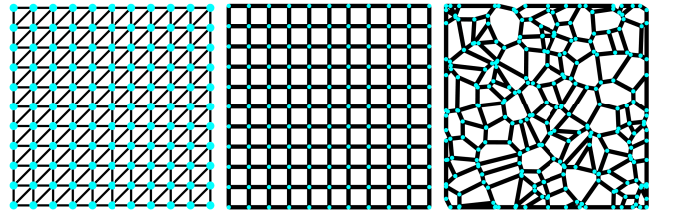


FIG. 2. Lattices used in the analysis, arranged from left to right: triangular, square, and Voronoi lattices.

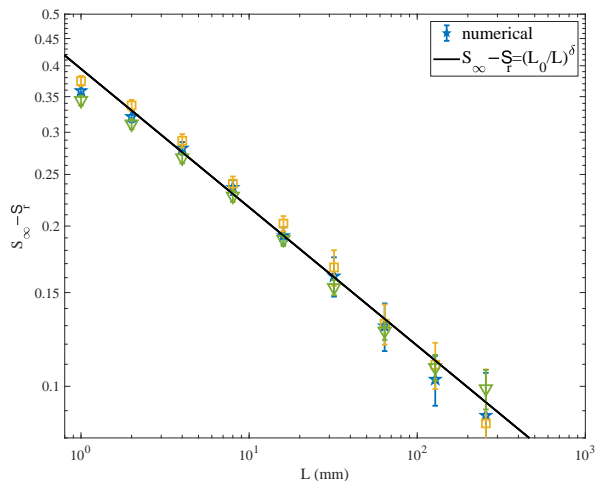


FIG. 3. Residual saturation versus lattice size for triangular (triangles), square (squares), and Voronoi (stars) lattices. $S_r(L)$ denotes the residual saturation for the lattice size L , while S_∞ is the statistical limit of the residual saturation when $L \rightarrow \infty$. The fitted power law is given by Eq. 3.

This algorithm differs from other IP algorithms that use the shortest-path algorithm [17, 18] in Step 4. In fully dynamics situations, the invaded fluid may choose the shortest path of the allowed pore space. This is different in the quasistatic limit, where all allowed pore spaces connected to the invaded zone can be invaded. This condition has been validated using the PMM [15]. The computational complexity of the shortest-path algorithm is $O(N \log N)$ [17], while the algorithm proposed here is $O(zN)$. The proposed algorithm also presents sleek advantages over other methods for multiphase flow in porous media, such as the lattice Boltzmann method [19], the level-set computational fluid dynamics [20], and pore morphology methods [15]. This is because the method is quasistatic, mesh-free, pixel-free, and has an unprecedented reduction of the computational complexity since the operations are performed in the extremely reduced dataset—the graph of the pore network.

Some snapshots of a simulation with a square lattice are shown in Fig. 1. The upper nodes are connected to the injection zone and the lower one with the evacuation zone. The first stage of the simulation corresponds to the subcritical regime ($p < p_c$), which is characterized by slow growth of the invaded region with minimal trapping. The percolation transition occurs near p_c and marks the point where the percolation occurs. After percolation, a short regime is detected, starting with the growth of the initial invaded percolation cluster and ending when the invaded cluster is fully established, creating a subnetwork where the flow of invaded fluid is fully established. The final stage is characterized by a slow filling of the invaded and trapped fluid that ends with a residual saturation, that is, the final saturation of the resident fluid: $S_r = 1 - S_I^{final} > 0$. Note that both critical percolation p_c and

residual saturation S_r are calculated directly from the graph, making them topological invariants. They depend only on the topology of the network and are independent of its geometry or the material properties of the solid matrix and fluids.

Similar finite-size effects as in BP are observed in our simulations. The percolation transition becomes sharper as the graph size increases, which is a characteristic of critical systems. In addition, strong statistical fluctuations in the residual saturation are observed from sample to sample, so a large number of simulations with the same parameters set are required to achieve averaged representative pressure-saturation curves. An extensive set of simulations was performed using three different networks: square, triangular, and Voronoi; see Figure 2. These lattices have a well-known BP threshold [6, 7, 21], a well-defined coordination number, and belong to the same universality class; see Table I. To examine the dependence of the pressure-saturation relations on the lattice size, we varied it as $L = 10 \times 2^n$, where $n = 0, 1, \dots, 8$. For each case, simulations were performed on 960 random realizations. In each realization, the throat radii were generated using a log-normal distribution. After simulations, the averaged values and standard errors were calculated.

The relation between residual saturation and lattice size is shown in Fig. 3. For all cases, the same power-law exponent $\delta = 0.26 \pm 0.005$ is obtained, suggesting it as a universal exponent within the universality class of regular two-dimensional networks. The exponent is significantly small, indicating strong size-dependency effects and a slow convergence to the statistical limit. The best fit for the residual saturation is given by

$$S_r(L) \approx S_\infty - \left(\frac{L_0}{L}\right)^\delta, \quad (3)$$

where $S_\infty = 0.53 \pm 0.02$ is the statistical limit of the residual saturation of the resident fluid, and $L_0 = 0.2 \pm 0.1$. Based on residual saturation, normalized saturation $s(p, L)$ is defined as the order parameter of the percolation process. This is expressed in terms of the lattice site L and the occupancy probability p

$$s(L) = \frac{1 - S(L)}{1 - S_r(L)}, \quad (4)$$

where $S(L)$ is the saturation of the resident fluid and $S_r(L)$ is its residual saturation. In percolation theory, the standard procedure involves performing a finite-size scaling analysis of the relation between the order parameter s and the control parameter p for values close to the critical percolation p_c where a behavior $s \sim |p - p_c|^{-\alpha}$ is expected as $p \rightarrow p_c$. The s - p curves for different lattice sizes are shown in Fig. 4a. The curves suggest self-similar solutions in the subcritical ($p < p_c$) and supercritical ($p > p_c$) regimes, with a clear asymmetry in both solutions. To find the self-similar solutions, an asymptotic

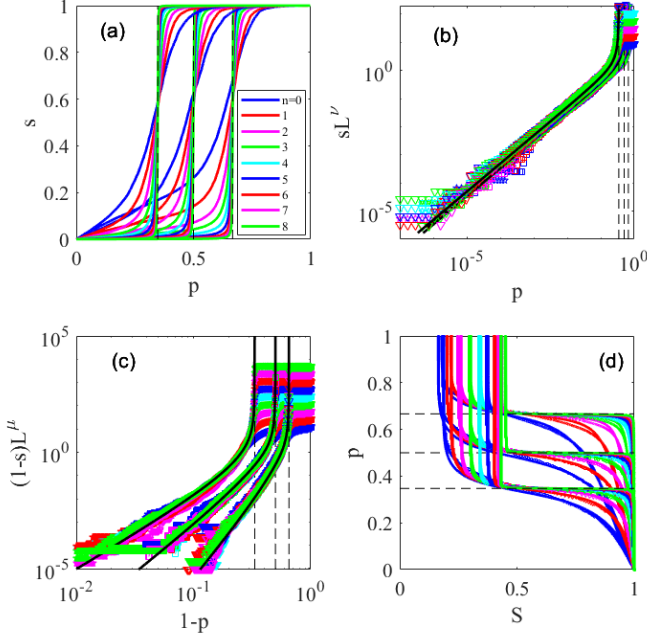


FIG. 4. Results from the finite-size scaling analysis of percolation: (a) Normalized saturation s versus occupancy probability p for different lattice sizes $L = 10 \times 2^n$, where $n = 0, 1, \dots, 8$. The lattices correspond to those shown in Fig. 2. As L increases, the percolation threshold manifests as a sharp phase transition at $p_c \approx 0.35, 0.5$, and 0.66 for triangular, square, and Voronoi lattices, respectively. (b) sL^ν versus p for all values of L , demonstrating data collapse across all lattice sizes for triangular (triangles), square (squares), and Voronoi (stars) lattices. (c) $(1-s)L^\mu$ versus $1-p$ for all lattice sizes, with data collapse depending on the coordination number of each lattice. (d) The uniform saturation $S = 1 - s(1 - S_r)$ calculated from the numerical data (symbols) and the analytical solution of Eq. 7 (solid lines). The dashed lines indicate the classical bond percolation (BP) threshold.

matching analysis is proposed: first, by finding the scaling relations in each regime, and then by asymptotically matching the solutions.

For the inner, or subcritical, solution, ($p < p_c$), the following scaling law is proposed

$$s = \frac{f(p)}{L^\nu(p - p_c)^\alpha}, \quad p < p_c \quad (5)$$

The outer, or supercritical solution ($p > p_c$), is expected to satisfy:

$$1 - s = \frac{g(1 - p)}{L^\mu(p - p_c)^\beta}, \quad p > p_c \quad (6)$$

Figs. 4(b-c) show a very good collapse of the data in the sub/super critical regimes. The exponents are determined as follows: The exponents ν and μ are optimized to achieve the best collapse of the curves s/L^ν and $(1-s)/L^\mu$ in the respective regimes. Then the exponents α and β are the minimal positive values that eliminate

the singularity of the self-similar functions $f(x)$ and $g(x)$ at $p = p_c$. The calculated exponents are $\nu = 0.92 \pm 0.02$, $\mu = 1.08 \pm 0.2$, $\alpha = 1.13 \pm 0.02$, and $\beta = 1.35 \pm 0.02$. These exponents are consistent across all three lattice topologies examined in this study, suggesting that they are universal within the universality class of regular two-dimensional lattices.

The self-similar scaling functions $f(x)$ and $g(x)$, on the other hand, are lattice-dependent and should be estimated from the collapsed curves. It is observed that $f(p) \sim p$ as $p \rightarrow 0^+$ and $g(1-p) \sim (1-p)^z$ as $p \rightarrow 1^-$, where z is the coordination number of the lattice. The self-similar function $f(x)$ is approximated as the Taylor expansion around $p = 0$ and the function $g(p)$ is approximated using the power expansion of x^z around $p = 1$. The exponents of Taylor expansions are calculated using the pressure-saturation relation of the largest lattice, which has size $L = 10 \times 2^8 = 2560$. The results shown in Table I, suggest that $g(x)$ is clearly non-universal since it depends on the coordination number of the lattice. The collapse of the curves into $f(x)$ in Figure 4b signals universality, however, whether $f(x)$ itself is universal remains inconclusive based on the data presented in Table I.

The last steps of the scaling analysis is the asymptotic matching. Eq. 5 defines p implicitly in terms of s as $p = p_{inner}(s)$. In the same way, p is implicitly given in terms of s from Eq. 6, which is expressed as $p = p_{outer}(s)$. The uniform solution is then obtained by asymptotic matching

$$p_{unif} = p_{inner} + p_{outer} - p_c. \quad (7)$$

The matching solution is compared with the numerical data in Fig. 4(d). An excellent agreement between the numerical results and the self-similar closed-form solution is achieved. Interestingly, these solutions consider only the classical bond percolation threshold p_c , and do not account for the backbone percolation transition discussed in the literature [22].

In summary, the quasistatic invasion percolation (IP) is formulated on the undirected graph of the pore network, using normalized saturation as the order parameter. Two topological invariants are detected: the percolation transition and residual saturation. The pressure-saturation relation is derived by scaling analysis, where all power-law exponents are universal. In contrast, the self-similar functions in the supercritical state are nonuniversal, as they depend on the coordination number of the lattice. The closed-form pressure-saturation relation is expressed in terms of four universal exponents. The topological invariance and the universality of the power-law exponents are particularly significant, as they enable the formulation of general laws that do not depend on the geometry of the porous medium or the material properties. The occupation probability is explicitly given as a function of the capillary pressure, the cumulative distribution function of the throat radii, and the material parameters of the solid-liquid-liquid interfaces (interfacial

Lattice	p_c	z	a1	a2	a3	b1	b2	b3
Voronoi	0.666	3	2.38 ± 0.05	-3.5 ± 0.1	0.002 ± 0.0005	2.06 ± 0.03	-12 ± 2	-100 ± 40
Square	0.5	4	1.53 ± 0.02	-2.2 ± 0.1	0.0004 ± 0.00006	2.39 ± 0.01	-30.5 ± 0.5	200 ± 10
Triangular	0.3473	6	1.48 ± 0.03	-2.8 ± 0.1	0.00026 ± 0.00003	1.81 ± 0.01	-22 ± 0.5	113 ± 3

TABLE I. Bond percolation threshold p_c , coordination number z , and coefficient of the Taylor expansion of the self-similar functions of the pressure-saturation relationships for different lattices. The expansions are given by $f(x) = a_1x + a_2x^2 + a_3x^3$ and $g(x) = b_1x^z + b_2x^{2z} + b_3x^{3z}$. The dependency of these functions on coordination number indicates that they are non-universal.

tension and contact angle). Consequently, this formulation provides an analytical derivation of the pressure-saturation relationship from first principles.

An outstanding issue is the slow convergence of the residual saturation to the statistical limit. This has implications on the finite-size effects on the representative element volumes (REV) used to obtain the constitutive relations for large-scale simulations. From Eq. 3, the deviation of the residual saturation from its statistical limit is given by $\Delta S \sim L^{-0.26}$. This means that to reduce this deviation by 50%, the REV size must be increased 14 times! This poses a serious question about the way

we perform large-scale simulations. These simulations are based on the assumption that the constitutive relations at each grid point are obtained from REV that are large enough to avoid size effects. However, these effects can only be removed by REV sizes larger than the grid size required to obtain accurate results, establishing a fundamental limit in the accuracy of these simulations. New light on this fundamental issue can be gained by the analysis of other networks, such as 3D, space-correlated, multiscale, and small-world networks.

Acknowledgments: The author thanks Morteza N. Najafi for useful discussions.

-
- [1] L. Furuberg, J. Feder, A. Aharony, and T. Jøssang, Dynamics of invasion percolation, *Physical review letters* **61**, 2117 (1988).
 - [2] A. G. Hunt and M. Sahimi, Flow, transport, and reaction in porous media: Percolation scaling, critical-path analysis, and effective medium approximation, *Reviews of Geophysics* **55**, 993 (2017).
 - [3] S. Assouline, D. Tessier, and A. Bruand, A conceptual model of the soil water retention curve, *Water Resources Research* **34**, 223 (1998).
 - [4] J. Shao, S. Havlin, and H. E. Stanley, Dynamic opinion model and invasion percolation, *Physical review letters* **103**, 018701 (2009).
 - [5] D. Wilkinson and J. F. Willemsen, Invasion percolation: a new form of percolation theory, *Journal of physics A: Mathematical and general* **16**, 3365 (1983).
 - [6] H. Kesten, The critical probability of bond percolation on the square lattice equals 1/2, *Communications in Mathematical Physics* **74**, 41 (1980).
 - [7] M. Sykes and J. Essam, Some exact critical percolation probabilities for bond and site problems in two dimensions, *Physical Review Letters* **10**, 3 (1963).
 - [8] H. J. Herrmann, D. Hong, and H. Stanley, Backbone and elastic backbone of percolation clusters obtained by the new method of 'burning', *Journal of Physics A: Mathematical and General* **17**, L261 (1984).
 - [9] K. Humphry, B. Suijkerbuijk, H. Van Der Linde, S. Pieterse, and S. Masalmeh, Impact of wettability on residual oil saturation and capillary desaturation curves, *Petrophysics* **55**, 313 (2014).
 - [10] F. Wolf, D. Siebert, and R. Surmas, Influence of the wettability on the residual fluid saturation for homogeneous and heterogeneous porous systems, *Physics of Fluids* **32** (2020).
 - [11] V. H. Nguyen, A. P. Sheppard, M. A. Knackstedt, and W. V. Pinczewski, The effect of displacement rate on imbibition relative permeability and residual saturation, *Journal of Petroleum Science and Engineering* **52**, 54 (2006).
 - [12] M. A. Knackstedt, M. Sahimi, and A. P. Sheppard, Nonuniversality of invasion percolation in two-dimensional systems, *Physical Review E* **65**, 035101 (2002).
 - [13] M. J. Blunt, *Multiphase flow in permeable media: A pore-scale perspective* (Cambridge university press, 2017).
 - [14] A. Heiba, M. Sahimi, L. Scriven, and H. Davis, Percolation theory of two-phase relative permeability, *SPE reservoir engineering* **7**, 123 (1992).
 - [15] M. Hilpert and C. T. Miller, Pore-morphology-based simulation of drainage in totally wetting porous media, *Advances in water resources* **24**, 243 (2001).
 - [16] F. Alonso-Marroquin and M. P. Andersson, Capillary pressure-saturation relation derived from the pore morphology method, Submitted to *Phys. Rev. E*, arXiv preprint arXiv:2501.07355 (2025).
 - [17] A. P. Sheppard, M. A. Knackstedt, W. V. Pinczewski, and M. Sahimi, Invasion percolation: new algorithms and universality classes, *Journal of Physics A: Mathematical and General* **32**, L521 (1999).
 - [18] D. Wilkinson, Percolation effects in immiscible displacement, *Physical Review A* **34**, 1380 (1986).
 - [19] K. Connington and T. Lee, A review of spurious currents in the lattice boltzmann method for multiphase flows, *Journal of mechanical science and technology* **26**, 3857 (2012).
 - [20] E. Olsson and G. Kreiss, A conservative level set method for two phase flow, *Journal of computational physics* **210**, 225 (2005).
 - [21] A. M. Becker and R. M. Ziff, Percolation thresholds on two-dimensional voronoi networks and delaunay triangulation.

- lations, Physical Review E—Statistical, Nonlinear, and Soft Matter Physics **80**, 041101 (2009).
- [22] C. I. Sampaio Filho, J. S. Andrade Jr, H. J. Herrmann, and A. A. Moreira, Elastic backbone defines a new transition in the percolation model, Physical review letters **120**, 175701 (2018).